

# Cavity-Enhanced IR Absorption in Planar Chalcogenide Glass Microdisk Resonators: Experiment and Analysis

Juejun Hu, Nathan Carlie, Laeticia Petit, Anu Agarwal, Kathleen Richardson, and Lionel C. Kimerling, *Member, IEEE*

**Abstract**—Planar microdisk optical resonators fabricated from  $\text{Ge}_{23}\text{Sb}_7\text{S}_{70}$  chalcogenide glass on a silicon substrate are applied for cavity-enhanced spectroscopic measurement of chemical molecular absorption fingerprint. A  $0.02 \text{ cm}^{-1}$  detection limit for these devices is demonstrated. This detection limit represents a threefold improvement as compared to a straight waveguide sensor, while the physical device length is reduced by 40-fold. The reduction in device footprint with enhanced sensitivity makes the structure attractive for “sensor-on-a-chip” device applications. We also present a design optimization approach for cavity-enhanced IR absorption spectroscopy using traveling-wave resonators, which indicates that further performance improvement can be achieved in optimally coupled, low-loss resonant cavities.

**Index Terms**—Amorphous materials, chemical analysis, glass, IR spectroscopy, integrated optics, microresonators, optical resonators, sulfur compounds.

## I. INTRODUCTION

PERHAPS the most widely used method of applied spectroscopy, IR absorption spectroscopy probes the characteristic vibration spectra of molecular species, and provides a wealth of structural and chemical information. This unique capability of IR spectroscopy has led to numerous applications in environmental monitoring [1], medical diagnosis [2], forensic analysis [3], and pharmaceutical manufacturing [4].

Traditional IR spectrophotometers usually employ a free-space geometry to measure single-pass absorbance. Such a configuration, however, poses a tradeoff between sensitivity and instrument footprint, since the sensitivity gain has to be achieved via increasing optical path length. Such a constraint can be overcome by using a resonant cavity (optical resonator), which offers resonantly-enhanced, long optical path length while still maintaining a small physical device size [5]–[7]. Compared to Fabry–Perot resonant cavities comprised of a pair of highly reflective mirrors, planar resonators, such as microrings and microdisks, do not require complicated

optical alignment, and can be mass produced at very low cost via mature planar CMOS microfabrication technologies. To date, cavity-enhanced absorption spectroscopy has only been demonstrated in silicon microring resonators [8]. The operation wavelength selection of such devices is bounded by the limited IR transparency window of the semiconductor materials used. Although the absorption fingerprints of most molecular species lie in the midwave and long-wave IR (wavelength  $> 3 \mu\text{m}$ ), cavity-enhanced spectroscopy in these wavelength range remains largely unexplored due to the limited material choice.

Chalcogenide glasses (ChGs), namely the amorphous compounds containing S, Se, and/or Te, have been recognized as a material of choice for IR applications due to their wide optical transparency in the midwave and long-wave IR [12]. Optical transmittance spectra of several chalcogenide glass compositions are shown in Fig. 1, along with those of silica and silicon for comparison. The wide IR transparency window of ChGs covers the characteristic absorption wavebands for most molecules of interest. Integrated chalcogenide glass waveguides operating in the midIR wavelength range have been demonstrated [13], [14], validating our material choice. Further, their amorphous nature allows ChG glass film deposition on virtually any substrate using low-cost, large-area techniques such as evaporation and sputtering. Lastly, sidewall roughness on as-fabricated chalcogenide-glass-guided wave photonic devices can be effectively removed to achieve low optical loss, a unique advantage over crystalline materials [15].

In this paper, we present the fabrication and characterization of planar microdisk resonators in Ge–Sb–S chalcogenide glass for optofluidic cavity-enhanced IR spectroscopy. Optofluidic integration is achieved via hybrid integration of the chalcogenide resonators with polydimethylsiloxane (PDMS) microfluidic channels for analyte transport. Using this device, we measure the optical absorption of *N*-methylaniline solutions in carbon tetrachloride ( $\text{CCl}_4$ ) at different concentration. We also discuss optical resonator design optimization for cavity-enhanced IR spectroscopy.

## II. THEORY

The transmission spectra through a waveguide-coupled resonant cavity can be generically derived using two mathematically equivalent approaches: the coupled mode theory [16] or the generalized coupling matrix formalism [17]. When the resonant condition is met, the power transmission coefficient  $T$  (in

Manuscript received May 04, 2009; revised July 30, 2009. First published August 25, 2009; current version published October 09, 2009. This work was supported in part by the Department of Energy under Award DE-SC52-06NA27341.

J. Hu, A. Agarwal, and L. C. Kimerling are with the Massachusetts Institute of Technology, Cambridge, MA 02139, USA (e-mail: hujuejun@mit.edu; anu@mit.edu; lckim@mit.edu).

N. Carlie, L. Petit, and K. Richardson are with the Clemson University, Clemson, SC 29634 USA (e-mail: ncarlie@clemson.edu; lpetit@clemson.edu; richar3@clemson.edu).

Digital Object Identifier 10.1109/JLT.2009.2030899

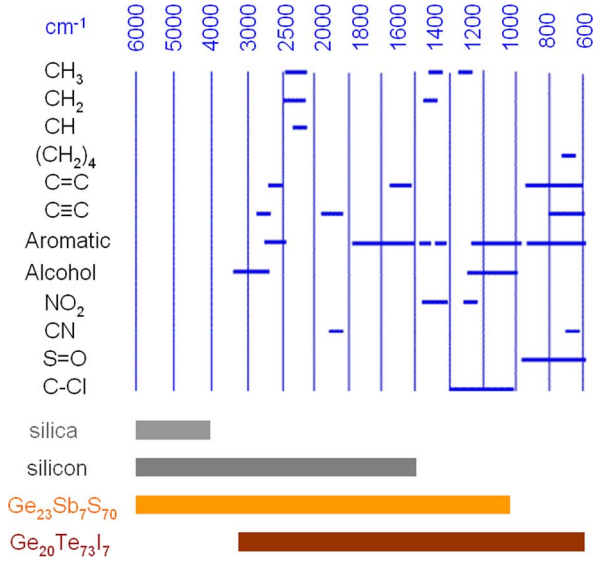


Fig. 1. (Top) IR absorption overtones of some common chemical species, represented by the horizontal lines [9]; (bottom) bars denote the optical material transparency window (defined as wavelength range where the material loss  $< 2$  dB/cm) of IR grade fused silica, silicon [10], as well as two chalcogenide glass compositions  $\text{Ge}_{23}\text{Sb}_7\text{S}_{70}$  and  $\text{Ge}_{20}\text{Te}_{73}\text{I}_7$  [11]. The two figures are aligned in wave numbers to facilitate comparison. It is clear the optical transparency window of ChGs covers most of the IR molecular absorption bands.

decibels) measured from the output end of the bus waveguide can be written as

$$T(\text{dB}) = 10 \log_{10} \frac{(\sqrt{A_i A_e} - \sqrt{1 - |k|^2})^2}{(1 - \sqrt{A_i A_e} \cdot \sqrt{1 - |k|^2})^2}$$

where  $k$  is the amplitude coupling coefficient from the bus waveguide to the resonator,  $A_i A_e$  represents round-trip transmission coefficient around the resonator (i.e.,  $1 - A_i A_e$  corresponds to the round-trip fractional energy loss inside the resonator), and the contributions from intrinsic resonant cavity optical loss and analyte solution absorption are denoted as  $A_i$  and  $A_e$ , respectively. The intrinsic linear optical loss  $\alpha_i$  in a resonator of physical length  $L$  is related to  $A_i$  by

$$\alpha_i = -\frac{1}{L} \ln A_i.$$

The values of  $k$  and  $A_i$  can be analytically solved using the generalized coupling matrix approach from the transmission spectra of the resonator in pure solvent <sup>1</sup>. Since the refractive index change from pure solvent to analyte solution is relatively small in our experiment ( $\Delta n < 0.01$ ), the coupling coefficient  $k$  can be practically regarded as a constant. The experimentally fitted  $k$  values typically differ by less than 2% before and after analyte solution injection in our tests, which confirms this assumption.

The additional optical loss due to introduction of analyte  $\alpha_e$  can be solved by linearizing the previous equation near  $\Delta T = 0$

$$A_e = 1 - 0.23 \cdot \left[ \frac{(A_i + 1) \cdot \sqrt{1 - |k|^2} - 2\sqrt{A_i}}{\sqrt{A_i} \cdot |k|^2} + 1 \right] \cdot \Delta T$$

<sup>1</sup>Note that the coupling regime in which the resonator operates (under-coupling or over-coupling) can be experimentally determined by comparing the extinction ratio evolution as a function of wavelength

where  $\Delta T$  is the change of resonant peak extinction ratio in decibels. The linear optical extinction coefficient  $\alpha_e$  of the analyte solution can then be analytically represented as

$$\begin{aligned} \Gamma \cdot \alpha_e &= -\frac{1}{L} \ln A_e \\ &= 0.23 \cdot \frac{1}{L} \\ &\quad \cdot \left[ \frac{(A_i + 1) \cdot \sqrt{1 - |k|^2} - 2\sqrt{A_i}}{\sqrt{A_i} \cdot |k|^2} + 1 \right] \cdot \Delta T \\ &= \frac{1}{S} \cdot \Delta T \end{aligned}$$

where

$$S = 0.434 \cdot L \cdot \left[ \frac{\sqrt{A_i} \cdot |k|^2}{(A_i + 1) \cdot \sqrt{1 - |k|^2} + \sqrt{A_i} \cdot (|k|^2 - 2)} \right]$$

where  $\Gamma$  denotes the confinement factor in the solution [19], which can be numerically computed based on the resonator dimensions.

The earlier equations correlate the absorption coefficient of solution  $\alpha$  with the experimental observable  $\Delta T$ . The factor  $\Gamma \cdot S$  can be defined as the “effective sensitivity” of the device, which specifies the extinction ratio change per unit solution absorption increase. Therefore, we can infer from the equations that three factors contribute to detection limit improvement of resonator absorption sensors: fine resolution of extinction ratio change  $\Delta T$ , high optical confinement  $\Gamma$  in the solution, and a large  $S$  factor which parametrically depends on intrinsic and extrinsic optical loss of the resonator ( $\alpha_i$  and  $k$ , respectively).

Based on the discussion, here, we use Monte Carlo simulations to quantitatively evaluate cavity-enhanced sensor design optimization towards improved detection limit of optical absorption in solutions. We note that even relatively small refractive index change in the solution leads to significant resonant wavelength shift, usually in a short time frame determined by the liquid flow rate in microfluidic channels (typically  $< 10$  s in our tests). For example, even a refractive index change of 0.001 can lead to a resonant wavelength shift in the order of 1 nm ( $\sim 200$  GHz), almost 100 times that of the resonant peak 3 dB bandwidth. Such a large peak shift can pose a challenge to active locking of the probing wavelength to the resonant peak. Further, accurate aligning of the probing wavelength to the exact resonant wavelength can be technically difficult in high- $Q$  resonators given the narrow spectral width of resonance. Instead, we adopt a wavelength interrogation scheme in our simulations and experiments. In a sensor measurement, transmission spectra of the resonator are monitored *in situ*, and the resonant peak extinction ratio is tracked to detect the presence of optical absorption in the solution. In a typical step spectral scan, the transmission spectrum actually consists of data points at discrete wavelength values, usually evenly spaced by a step size  $\Delta \lambda_s$ . In order to simulate the impact of measurement noise in this wavelength-interrogation process, a Monte Carlo approach is employed to predict the resolution of extinction ratio change  $\Delta T$ . Randomly generated Gaussian-type white noise is superimposed onto the spectral data points calculated using a generalized coupling matrix method. We then perform a Lorentzian fit

to the data points in a linear scale near a resonant peak to extract the peak parameters including extinction ratio. The minimum resolvable extinction ratio change  $\Delta T_{\min}$  is statistically defined as the ensemble average of deviations of the “measured” values from the actual resonant wavelength over 1000 Monte Carlo iterations. Relative numerical error arising from the random nature of the Monte Carlo method was estimated to be  $\sim \pm 5\%$ . More details of the simulation method are described elsewhere [20]. Since the factor  $S$  and confinement factor  $\Gamma$  can be calculated using given device parameters, the detection limit of solution optical absorption  $\alpha$  can be calculated by substituting the simulated  $\Delta T_{\min}$  value into the equations derived earlier.

Our simulations indicate that there are four factors affecting the detection limit of resonant cavity-enhanced optical absorption sensors, represented by  $\Gamma \cdot \alpha$ , the product of confinement factor in the solution, and the minimum detectable solution optical absorption to achieve a signal-to-noise ratio of unity: the wavelength step  $\Delta \lambda_s$  used in a spectral scan across the resonant peak; the SNR of resonator transmission measurements at each discrete wavelength point, which is proportional to the square root of integration time in a white noise limit; the intrinsic linear optical loss inside the resonator (e.g., due to roughness scattering or absorption of the resonator material); and the ratio between extrinsic loss (i.e., cavity loss arising from coupling to bus waveguides) and the intrinsic optical loss. The former two factors are related to the measurement instrumentation, whereas the latter two are intrinsic properties of the optical resonator.

According to the simulation results, the detection limit  $\Gamma \cdot \alpha$  of absorption sensors is proportional to the square root of the spectral scan wavelength step  $\Delta \lambda_s$ . Intuitively, spectral scans with fine wavelength steps provide a more accurate description of the transmission spectra, and hence, smaller  $\Delta T_{\min}$ ; more rigorous analysis shows that this is a direct consequence of the white noise distribution used in our Monte Carlo simulations, an assumption that holds for most types of noise sources in a spectral measurement.

The detection limit  $\Gamma \cdot \alpha$  of absorption sensors is also inversely proportional to the transmission measurement SNR. This result suggests that improved sensor detection limit can be achieved through suppressing noise in the resonator transmission spectrum measurement, for example, by using light source with superior power stability and read-out electronics with reduced circuit noise.

Fig. 2 plots the simulated detection limit of  $\Gamma \cdot \alpha$  as functions of the intrinsic resonator loss and the ratio between extrinsic and intrinsic loss in two different regimes: (a) under-coupling and (b) over-coupling. In the Monte Carlo simulations we assume an SNR of 20 dB for transmission measurements at each discrete wavelength and a spectral scan step of 1 pm. The detection limit of sensors with different measurement instrumentation parameters can thus be calculated according to the proportionality relations described earlier. As we can see from the plots, resonators with low intrinsic loss and a medium extrinsic loss to intrinsic loss ratio (corresponding to an extinction ratio of  $\sim 12$  dB) gives the lowest detection limit, and hence, an optimal sensor design. This optimal extinction ratio value arises from the tradeoff between maximizing the  $S$  factor and improving the extinction ratio change resolution  $\Delta T_{\min}$ : although resonant

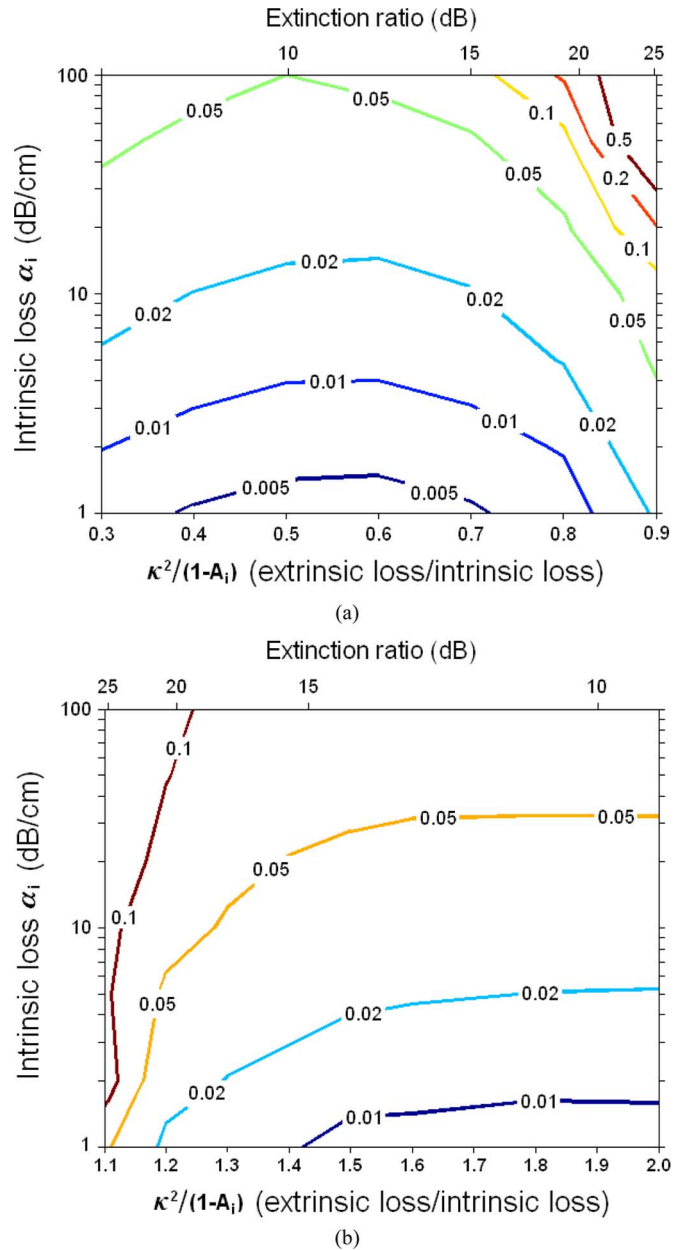


Fig. 2. Detection limit  $\Gamma \cdot \alpha$  of optical resonator sensors simulated using a Monte Carlo approach. The vertical axis represents the intrinsic linear optical loss inside the resonator, the horizontal axis is the ratio between round-trip extrinsic loss (coupling loss)  $k^2$  and intrinsic loss  $1 - A_i$ , and the detection limit values of  $\Gamma \cdot \alpha$  can be read out from the isoresolution curves (in centimeters inverse). When  $k^2/(1 - A_i) < 1$ : (a) resonator is under-coupled, and when  $k^2/(1 - A_i) > 1$ : (b) resonator is over-coupled. The simulation assumes an SNR of 20 dB for transmission measurements at each discrete wavelength and a spectral scan step of 1 pm. Notably, as the sensor detection limit scales linearly with noise amplitude, the detection limit of sensors with an arbitrary SNR can be calculated using the figures through the scaling rule.

peaks with a high extinction ratio show more sensitive response to changes in optical absorption (i.e., larger  $\Delta T$  for the same optical absorption in the solution  $\alpha_e$ ) [21], even small deviations in Lorentzian peak fit translate to a significant error of extinction ratio estimation. In addition, Fig. 2 suggests that under-coupled resonator sensors exhibit improved detection limit compared to over-coupled resonators with the same intrinsic loss figures, which possibly can be attributed to the lower extrinsic

loss, and hence, higher loaded cavity  $Q$ -factors of under-coupled resonators.

Lastly, it is worth noting that even though resonators are often considered as intrinsically narrowband devices, spectroscopic scans covering a wide wavelength range can be performed by simultaneous monitoring of multiple resonant peaks in cavity-enhanced spectroscopy. In this regard, the spectroscopic wavelength resolution is only limited by the free spectral range (FSR) of the resonator. Therefore, resonators with large radius are better suited for high-resolution spectroscopic applications given as their small FSR, and hence, closely packed resonant peaks.

To summarize, slightly under-coupled (extinction ratio  $\sim 12$  dB), low loss resonant cavities lead to superior detection limit of optical absorption in the solution.

### III. EXPERIMENT

#### A. Device Fabrication

Bulk  $\text{Ge}_{23}\text{Sb}_7\text{S}_{70}$  chalcogenide glass is prepared using a melt-quenching technique [21]. High-quality glass films are deposited on 6-in Si wafers (precoated with  $3\ \mu\text{m}$  thermal oxide; Silicon Quest International, Inc.) via single-source thermal evaporation from the glass bulks. The films are patterned by lift-off, with the complete patterning process realized on a 500-nm CMOS line. The film deposition process and lift-off fabrication are described in detail elsewhere [22], [24]. A “pulley-type” configuration is employed to increase waveguide-resonator coupling efficiency and improve device fabrication tolerance [23]. The bus waveguides are comprised of photonic wires with a width of 800 nm, and microdisks and bus waveguides both have a nominal height of 450 nm. We test different microdisks with radii of 20, 30, and 50  $\mu\text{m}$  for cavity-enhanced spectroscopy; the similar spectroscopic results obtained from the tests suggest excellent fabrication uniformity and reproducibility, as well as the general applicability of the spectroscopic device operation principle.

PDMS (Sylgard 184 Silicone Elastomer, Dow Corning, Inc.) microfluidic channels with a width of 100  $\mu\text{m}$  and a height of 30  $\mu\text{m}$  are fabricated via replica molding. After oxygen plasma treatment, the channels are irreversibly bonded onto the chips on which the microdisks are patterned. Liquid inlet and outlet access holes are punched prior to bonding, and polytetrafluoroethylene (PTFE) tubing is attached into the access holes to complete the microfluidic chip fabrication. A top view micrograph of the fabricated microfluidic channel overlaid with a linear array of Ge--Sb--S microdisks is shown in Fig. 3(a).

#### B. Cavity-Enhanced Spectroscopic Testing

We use the optofluidic resonator device to measure the well-defined absorption peak of *N*-methylaniline near 1500 nm [22]. The transmission spectra of the fabricated devices are measured on a Newport AutoAlign workstation in combination with a LUNA tunable laser (optical vector analyzer; LUNA Technologies, Inc.). The laser wavelength scanning step used in our tests is  $\sim 2.6$  pm. Multiple scan averaging is employed to reduce noise and improve measurement resolution. Lens-tip fibers are used to couple light from the laser into and out of the

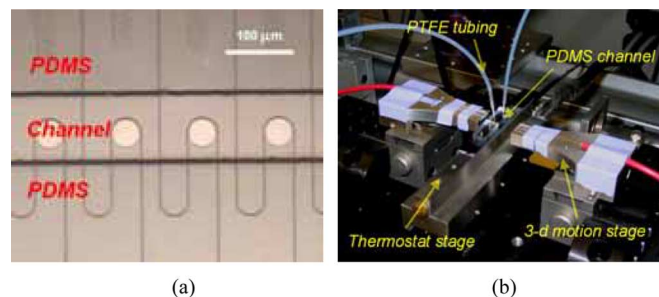


Fig. 3. (a) Top view: Micrograph of a PDMS microfluidic channel overlaid with a linear array of 20  $\mu\text{m}$  radius Ge--Sb--S microdisks. (b) Optofluidic chip under testing.

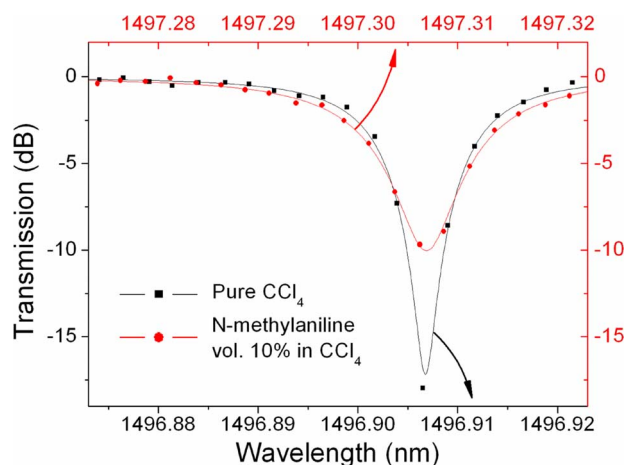


Fig. 4. Microdisk transmission spectra around a resonant peak before and after *N*-methylaniline solution injection: dots are experimentally measured data points and the lines are theoretical fitting results based on the generalized coupling matrix formalism; the extinction ratio change and resonant peak broadening are due to the optical absorption of *N*-methylaniline near 1500 nm. Note that the resonant wavelength red shifts due to the refractive index difference between pure  $\text{CCl}_4$  and *N*-methylaniline solution.

devices. Reproducible coupling is achieved via an automatic alignment system with a spatial resolution of 50 nm. The sample is mounted on a thermostat stage and kept at 25°C for all measurements. Fig. 3(b) shows a photograph of the optofluidic resonator device under testing. Prior to device testing using *N*-methylaniline solutions, transmission spectra of the resonators are measured when the microfluidic channels are filled with pure carbon tetrachloride. The “baseline” spectra are then used to derive intrinsic device parameters ( $\alpha_1$  and  $k$ ) of the resonators. Quality factors ( $Q$ ) of the resonators under testing is within the range of 130 000 ( $\pm 15\%$ ) in pure  $\text{CCl}_4$ , which corresponds to a linear waveguide loss of  $\sim 1.5$  dB/cm. During the cavity-enhanced spectroscopic test, *N*-methylaniline solutions in carbon tetrachloride of varying concentrations are injected into the channels using a syringe pump and the optical transmission spectra of the resonators are monitored *in situ*.

Fig. 4 shows the transmission spectra around a resonant peak, both before and after injection of 10 vol.% *N*-methylaniline solution in  $\text{CCl}_4$  into the microfluidic channel. The resonator works in an under-coupling regime; therefore the additional optical loss due to *N*-methylaniline absorption results in a decrease of the extinction ratio along with a broadening of the resonant peak.

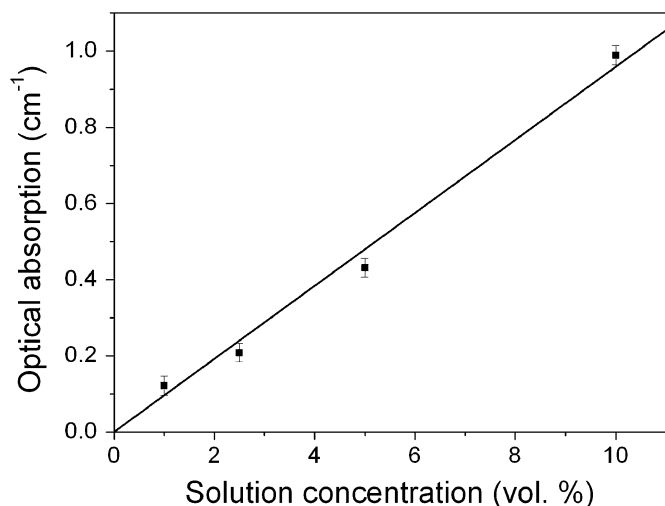


Fig. 5. Measured optical absorption of *N*-methylaniline solutions in carbon tetrachloride as a function of *N*-methylaniline concentration near the wavelength of 1500 nm.

Using the formula that we have presented in the previous section, the optical absorption of *N*-methylaniline solution can be extracted based on the resonant peak extinction ratio change. Fig. 5 plots the optical absorption of *N*-methylaniline solutions with different concentrations, measured using the optofluidic resonator. The lowest concentration we test in our experiment is 1%, which corresponds to  $\sim 0.1 \text{ cm}^{-1}$  absorption coefficient. To evaluate the absorption detection limit of the device, we performed multiple measurements and the standard deviation of the resulting data is taken as the noise floor of our experimental setup. If we define the detection limit as the solution optical absorption that generates a signal-to-noise ratio of unity, the detection limit of a resonator with 17.2 dB extinction ratio (see Fig. 4) is approximately  $0.02 \text{ cm}^{-1}$  based on experimentally determined noise floor. This is attained with 64 wavelength-sweeping scan averaging across the resonant peak and an effective 64-scan total integration time of 0.6 s. The  $0.02 \text{ cm}^{-1}$  detection limit is in good agreement with the theoretically simulated value of  $0.016 \text{ cm}^{-1}$ , using the Monte Carlo method. The experimentally measured detection limit in our tests represents an order of magnitude improvement over on-chip absorption spectroscopy using silicon microring resonators [8], mainly due to reduced instrument noise. Further, the present study result features a threefold improvement compared to our previous result attained with a straight waveguide sensor with centimeter-long optical path length ( $\sim 0.07 \text{ cm}^{-1}$ ) [24], while the physical device length is decreased by 40-fold. Such comparison clearly demonstrates the competitive advantage of using optical resonators for “sensor-on-a-chip” type IR absorption spectroscopy.

#### IV. CONCLUSION

In this paper, we demonstrate cavity-enhanced IR absorption spectroscopy using optofluidic microresonators in Ge--Sb--S chalcogenide glass. We achieve a detection limit of  $\sim 0.02 \text{ cm}^{-1}$  to optical absorption in *N*-methylaniline solutions, using microdisk resonators with a cavity  $Q$ -factor of  $\sim 130\,000$ . We show that slightly under-coupled (extinction ratio  $\sim 12 \text{ dB}$ ),

low-loss resonant cavities lead to optimized detection limit of optical absorption in the solution.

#### ACKNOWLEDGMENT

The authors would like to thank P. Mao and the Micro/Nanofluidic BioMEMS group at MIT for technical assistance and helpful discussions. The authors also acknowledge Microsystems Technology Laboratories at MIT and Center for Materials Science and Engineering at MIT for fabrication and characterization facilities.

This paper was prepared as an account of work supported by an agency of the United States Government. Neither the United States Government nor any agency thereof, nor any of their employees, makes any warranty, express or implied, or assumes any legal liability or responsibility for the accuracy, completeness or usefulness of any information, apparatus, product or process disclosed, or represents that its use would not infringe privately owned rights. Reference herein to any specific commercial product, process, or service by trade name, trademark, manufacturer, or otherwise does not necessarily constitute or imply its endorsement, recommendation, or favoring by the United States Government or any agency thereof. The views and opinions of authors expressed herein do not necessarily state or reflect those of the United States Government or any agency thereof.

#### REFERENCES

- [1] P. A. Martin, “Near-infrared diode laser spectroscopy in chemical process and environmental air monitoring,” *Chem. Soc. Rev.*, vol. 31, pp. 201–210, 2002.
- [2] S. Hocdé, O. Loréal, O. Sire, C. Boussard-Plédel, B. Bureau, B. Turlin, J. Keirsse, P. Leroyer, and J. Lucas, “Metabolic imaging of tissues by infrared fiber-optic spectroscopy: An efficient tool for medical diagnosis,” *J. Biomed. Opt.*, vol. 9, pp. 404–407, Mar. 2004.
- [3] R. Schneider and K. Kovar, “Analysis of ecstasy tablets: Comparison of reflectance and transmittance near infrared spectroscopy,” *Forensic Sci. Int.*, vol. 134, pp. 187–195, 2003.
- [4] G. Reich, “Near-infrared spectroscopy and imaging: Basic principles and pharmaceutical applications,” *Adv. Drug Del. Rev.*, vol. 57, pp. 1109–1143, Jun. 2005.
- [5] T. McGarvey, A. Conjusteau, and H. Mabuchi, “Finesse and sensitivity gain in cavity-enhanced absorption spectroscopy of biomolecules in solution,” *Opt. Exp.*, vol. 14, no. 22, pp. 10441–10451, Oct. 2006.
- [6] J. Nadeau, V. Ilchenko, D. Kossokovski, G. Bearman, and L. Maleki, “High-Q whispering-gallery mode sensor in liquids,” *Proc. SPIE*, vol. 4629, pp. 172–180, 2002.
- [7] G. Farca, S. Shopova, and A. Rosenberger, “Cavity-enhanced laser absorption spectroscopy using microresonator whispering-gallery modes,” *Opt. Exp.*, vol. 15, no. 25, pp. 17443–17448, Dec. 2007.
- [8] A. Nitkowski, L. Chen, and M. Lipson, “Cavity-enhanced on-chip absorption spectroscopy using microring resonators,” *Opt. Exp.*, vol. 16, no. 16, pp. 11930–11936, Jul. 2008.
- [9] R. P. Scott, *Tandem Techniques*, ser. (Separation Science Series). New York: Wiley, Mar. 1997.
- [10] G. J. Hawkins, “Spectral characterisation of infrared optical materials and filters,” Ph.D. dissertation, Dept. Cybern., Univ. Reading, Reading, U.K., 1998.
- [11] A. Wilhelm, C. Boussard-Plédel, Q. Coulombier, J. Lucas, B. Bureau, and P. Lucas, “Development of far-infrared-transmitting Te based glasses suitable for carbon dioxide detection and space optics,” *Adv. Mater.*, vol. 19, no. 22, pp. 3796–3800, Oct. 2007.
- [12] J. Savage, “Optical properties of chalcogenide glasses,” *J. Non-Cryst. Solids*, vol. 47, pp. 101–115, 1982.
- [13] A. Ganjoo, H. Jain, C. Yu, J. Irudayaraj, and C. Pantano, “Detection and fingerprinting of pathogens: MidIR biosensor using amorphous chalcogenide films,” *J. Non-Cryst. Solids*, vol. 354, pp. 2757–2762, May 2008.

- [14] N. Hô, M. Phillips, H. Qiao, P. Allen, K. Krishnaswami, B. Riley, T. Myers, and N. Anheier, "Single-mode low-loss chalcogenide glass waveguides for the midinfrared," *Opt. Lett.*, vol. 31, pp. 1860–1862, Jun. 2006.
- [15] J. Hu, N. Carlie, N. Feng, L. Petit, A. Agarwal, K. Richardson, and L. C. Kimerling, "Optical loss reduction in HIC chalcogenide glass waveguides via thermal reflow," to be published.
- [16] B. E. Little, S. T. Chu, H. A. Haus, J. Foresi, and J.-P. Laine, "Microring resonator channel dropping filters," *J. Lightw. Technol.*, vol. 15, no. 6, pp. 998–1005, Jun. 1997.
- [17] A. Yariv, "Universal relations for coupling of optical power between microresonators and dielectric waveguides," *Electron. Lett.*, vol. 36, no. 4, pp. 321–322, Feb. 2000.
- [18] J. Robinson, L. Chen, and M. Lipson, "On-chip gas detection in silicon optical microcavities," *Opt. Exp.*, vol. 16, pp. 4296–4301, 2008.
- [19] J. Hu, X. Sun, A. Agarwal, and L. C. Kimerling, "Design guidelines for optical resonator biochemical sensors," *J. Opt. Soc. Amer. B*, vol. 26, pp. 1032–1041, 2009.
- [20] R. Boyd and J. Heebner, "Sensitive disk resonator photonic biosensor," *Appl. Opt.*, vol. 40, pp. 5742–5747, Nov. 2001.
- [21] L. Petit, N. Carlie, F. Adamietz, M. Couzi, V. Rodriguez, and K. C. Richardson, "Correlation between physical, optical and structural properties of sulfide glasses in the system Ge–Sb–S," *Mater. Chem. Phys.*, vol. 97, pp. 64–70, 2006.
- [22] J. Hu, V. Tarasov, N. Carlie, L. Petit, A. Agarwal, K. Richardson, and L. C. Kimerling, "Fabrication and testing of planar chalcogenide waveguide integrated microfluidic sensor," *Opt. Exp.*, vol. 15, pp. 2307–2314, Mar. 2007.
- [23] J. Hu, V. Tarasov, N. Carlie, N. Feng, L. Petit, A. Agarwal, K. Richardson, and L. C. Kimerling, "Si-CMOS-compatible lift-off fabrication of low-loss planar chalcogenide waveguides," *Opt. Exp.*, vol. 15, pp. 11798–11807, Sep. 2007.
- [24] J. Hu, N. Carlie, N. Feng, L. Petit, A. Agarwal, K. Richardson, and L. C. Kimerling, "Planar waveguide-coupled, high-index-contrast, high-Q resonators in chalcogenide glass for sensing," *Opt. Lett.*, vol. 33, pp. 2500–2502, Nov. 2008.

**Juejun Hu** received the B.Sc. degree in materials science and engineering from Tsinghua University, Beijing, China, in 2004. He is currently working toward the Ph.D. degree in materials science and engineering at Massachusetts Institute of Technology, Cambridge.

His current research interests include planar chalcogenide glass materials and devices, optical resonant cavity structures for sensing, optomechanics, and magneto-optics.

**Nathan Carlie**, photograph and biography not available at the time of publication.

**Laeticia Petit**, photograph and biography not available at the time of publication.

**Anu Agarwal**, photograph and biography not available at the time of publication.

**Kathleen Richardson** received the B.S. degree in ceramic engineering, the M.S. degree in glass science, and the Ph.D. degree in ceramics/glass science and engineering from the New York State College of Ceramics, Alfred University, Alfred, NY, in 1982, 1988, and 1992, respectively.

She is currently a Professor and the Director of the School of Materials Science and Engineering, Clemson University, Clemson, SC. She has authored or coauthored more than 120 refereed publications, reviews, proceedings, and book chapters, presented more than 225 invited and contributed presentations, and has organized and chaired numerous domestic and international meetings within her discipline. Her current research interests include the development and manufacturing science of IR glasses and glass ceramic materials.

Dr. Richardson is currently a Fellow in the Society of Glass Technology, the International Society for Optical Engineers, and the American Ceramic Society.

**Lionel C. Kimerling** (M'89) received the S.B. degree in metallurgical engineering and the Ph.D. degree in materials science from the Massachusetts Institute of Technology (MIT), Cambridge, in 1965 and 1969, respectively.

He was the Head of the Materials Physics Research Department, AT&T Bell Laboratories, Murray Hill, NJ. He is currently the Thomas Lord Professor of Materials Science and Engineering at MIT. In addition to his teaching duties in electronic, optical, and optoelectronic materials, he is the Director of the MIT Microphotonics Center. His current research interests include silicon processing that addresses photovoltaic cells, environmentally benign integrated circuit manufacturing, and monolithic microphotonic devices and circuits.